

# UIT: Ultraviolet Observations of the Small Magellanic Cloud

Robert H. Cornett<sup>1</sup> Michael R. Greason<sup>1</sup> Jesse K. Hill<sup>1</sup>

Joel Wm. Parker<sup>2</sup> William H. Waller<sup>1</sup>

Ralph C. Bohlin<sup>3</sup> Kwang-Peng Cheng<sup>4</sup> Susan G. Neff<sup>5</sup> Robert W. O'Connell<sup>6</sup>

Morton S. Roberts<sup>7</sup> Andrew M. Smith<sup>5</sup> and Theodore P. Stecher<sup>5</sup>

## ABSTRACT

A mosaic of four UIT far-UV (FUV) ( $\lambda_{eff} = 1620\text{\AA}$ ) images, with derived stellar and HII region photometry, is presented for most of the Bar of the SMC. The UV morphology of the SMC's Bar shows that recent star formation there has left striking features including: a) four concentrations of UV-bright stars spread from northeast to southwest at nearly equal ( $\sim 30$  arcmin= $0.5$  kpc) spacings; b) one of the concentrations, near DEM 55, comprises a well-defined 8-arcmin diameter ring surrounded by a larger H $\alpha$  ring, suggestive of sequential star formation.

FUV PSF photometry is obtained for 11,306 stars in the FUV images, resulting in magnitudes  $m(162)$ . We present a FUV luminosity function for the SMC bar, complete to  $m(162) \sim 14.5$ . Detected objects are well correlated with other SMC Population I material; of 711 H $\alpha$  emission-line stars and small nebulae within the UIT fields of view, 520 are identified with FUV sources. The FUV photometry is compared with available ground-based catalogs of supergiants, yielding 191 detections of 195 supergiants with spectral type earlier than F0 in the UIT fields. The  $(m(162) - V)$  color for supergiants is a sensitive measure of spectral type. The bluest observed colors for each type agree well with colors computed from unreddened Galactic spectral atlas stars

---

<sup>1</sup>Hughes STX Corporation, Code 681, Goddard Space Flight Center, Greenbelt MD 20771

<sup>2</sup>Southwest Research Institute, Boulder CO

<sup>3</sup>Space Telescope Science Institute, Homewood Campus, Baltimore, MD 21218

<sup>4</sup>Department of Physics, California State University, Fullerton, CA 92634

<sup>5</sup>Laboratory for Astronomy and Solar Physics, Code 680, Goddard Space Flight Center, Greenbelt MD 20771

<sup>6</sup>University of Virginia, Astronomy Department, P.O. Box 3818, Charlottesville, VA 22903

<sup>7</sup>National Radio Astronomy Observatory, Edgemont Rd., Charlottesville, VA 22903

for types earlier than about A0; for later spectral types the observed SMC stars range significantly bluer, as predicted by comparison of low-metallicity and Galactic-composition models. Redder colors for some stars of all spectral types are attributed to the strong FUV extinction arising from even small amounts of SMC dust. Internal SMC reddenings are determined for all catalog stars. All stars with  $E(B-V) > 0.15$  are within regions of visible  $H\alpha$  emission.

FUV photometry for 42  $H\alpha$ -selected HII regions in the SMC Bar is obtained for stars and for total emission (as measured in HII-region-sized apertures). The flux-weighted average ratio of total to stellar FUV flux is 2.15; consideration of the stellar FUV luminosity function indicates that most of the excess total flux is due to scattered FUV radiation, rather than stars fainter than  $m(162) = 14.5$ . Both stellar and total emission are well correlated with  $H\alpha$  fluxes measured by Kennicutt and Hodge (1986; hereafter KH), yielding FUV/ $H\alpha$  flux ratios that are consistent with models of SMC metallicity, ages from 1-5 Myr, and moderate ( $E(B-V) = 0.0-0.1$  mag) internal SMC extinction.

## 1. Introduction

UV observations from above the earth’s atmosphere are vital for understanding the Population I properties of metal-poor galaxies such as the Small Magellanic Cloud (SMC). Optical-band studies of the SMC have shown that this nearby dwarf irregular galaxy provides a unique laboratory for investigating stellar and interstellar evolution at “primitive” compositions, compared to the Galaxy. Many effects of composition differences appear best, or only, in the UV. Line blanketing strongly affects UV colors; similarly, the steep SMC extinction curve ( $A_{162}/E(B-V) \sim 16$ ), widely thought to be due to abundances in SMC dust, is “extreme” only in the UV. Moreover, because the energy distributions of hot stars peak at short wavelengths, FUV photometry is more effective than optical-band photometry in determining the temperatures of such stars. Here, we present initial results from a UV imaging study of the the SMC, based on a mosaic of four far-UV images that were obtained by the Ultraviolet Imaging Telescope (UIT) during the Astro-1 and Astro-2 missions in late 1990 and early 1995.

## 2. Observations and Data Reduction

UIT observed a total of four 40-arcmin diameter fields nearly completely covering the SMC Bar at an angular resolution of  $\sim 3$  arcsec– better than 75 times the resolution of

previous UV imaging studies of the SMC (Okumura 1993). A description of individual exposures used in this study is in Table 1, and a mosaic of the longest exposures for each field is shown as Figure 1. Details of UIT hardware, calibration, operations, and data reduction are in Stecher *et al.* 1992 and Stecher *et al.* 1996. Data discussed here are from images made with the  $\lambda_{eff}=1620\text{\AA}$  filter, hereafter called 'B5'. Astro-1 data also include short exposures of Field 1 made in a near-UV ( $\lambda_{eff}=2490\text{\AA}$ ) and an additional far-UV ( $\lambda_{eff}=1520\text{\AA}$ ) bandpass (cf Cornett *et al.* 1994) which are not discussed here. (A discussion and analysis of UIT imaging of the Large Magellanic Cloud is given in Parker *et al.* 1996.)

UIT film images are reduced to linearized arrays and absolutely calibrated by comparison to other UV spectrophotometry as described in Stecher *et al.* 1992. The calibration for Astro-2 data has been revised using flight observations of standard fields (Stecher *et al.* 1996); estimated absolute uncertainty is 15% for well-exposed pixels.

An IDL/UIT implementation of DAOPHOT (Stetson 1987; J.K.Hill *et al.* 1993) is used to locate stars and perform aperture and PSF-fit photometry. Both aperture and PSF-fit photometry use a 2.9-arcsec (2.5-pixel) radius, which sets the limit for resolution of blended stars and the minimum size for non-stellar sources. PSF-fit photometry, using parameters chosen for images individually, is used for subsequent analysis of stellar objects. Astrometric solutions are derived for UIT images using HST guide stars as standards (Lasker *et al.* 1989). 11306 stars are measured, and positions, magnitudes, and errors for these objects are provided in the AAS CD-ROM series. The file includes UIT star number, field number, x and y positions in UIT pixels, right ascension and declination,  $m(162)$  derived from PSF photometry, and estimated error in  $m(162)$ .

For the SMC data, IUE observations are used to measure combined aperture corrections and improved single-field absolute calibrations. The corrections are determined by integrating well-exposed and calibrated (Bohlin *et al.* 1990) IUE spectra of isolated field stars in each UIT image, and comparing the results with UIT PSF photometry. The number of IUE spectra used for each field ranges from 12 to 31. Statistical uncertainties in mean IUE/UIT ratios range from .07 to .02 mag, with larger uncertainties for longer UIT exposures because of the overexposure of the IUE sources on those images. The IUE/UIT ratio thus derived agrees with the nominal UIT absolute calibration within 10%, after application of a directly measured aperture correction. UIT magnitudes are defined by  $m_\lambda = -2.5 \log(F_\lambda) - 21.1$ , where  $F_\lambda$  is in  $\text{erg} (\text{cm}^2 \text{\AA} \text{ s})^{-1}$ .

Data from multiple exposures of each field are combined by selecting data from individual exposures which maximize the signal-to-noise ratio. For stellar images and pixels which are common to two fields, data are used from the field with the longer maximum exposure time, after signal-to-noise selection. In practice signal-to-noise selection is achieved

for stellar photometry by restricting each exposure to a selected stellar magnitude range; this avoids systematic errors at the extremes of the UIT dynamic range on single exposures. For photometry of non-stellar objects, an extended-dynamic-range, calibrated composite image is produced for each field by 1) boxaveraging all exposures to a  $\sim 4.5$  arcsec pixel size (to minimize the effects of possible densitometry misalignments of up to  $\sim 1.12$  arcsec), and 2) selecting and using pixels from the individual boxaveraged frames with exposure values which maximize signal-to-noise ratios. This composite image is subsequently used for all extended source photometry.

### 3. Far-UV Morphology

Figure 1 shows that FUV emission from the SMC originates mostly in hot stellar populations which, while not restricted to clusters, are significantly clumped. No diffuse FUV emission is readily apparent (but see Section 5). The brightest features in the UIT images are the clusters NGC 346 and NGC 330, with additional FUV concentrations approximately centered in fields 1 and 2. The bright FUV concentrations, spaced along the Bar centered at  $\sim 0.5$  kpc intervals, have similar clustering and distribution properties to those evident in wide-field FUV images of the LMC (Smith, Cornett, and Hill 1987).

Comparison of large-scale  $H\alpha$  and FUV morphologies (Figure 2 a) and b)); Bothun, personal communication) can reveal spatial and temporal sequences of star formation over timescales of  $\sim 20$  Myr (R.S.Hill *et al.* 1994). Ionized hydrogen emission marks the locations of the earliest-type stars, while detectible FUV flux is emitted by stars as late as A0. Therefore,  $H\alpha$  is strong for clusters up to a few million years of age, while detectible FUV emission continues for about 20 Myr. Figures 2a) and b) show that FUV concentrations cover a range of ages, including cases with coincident bright young  $H\alpha$  sources at the NE and SW ends of the bar, as well as evolved regions without  $H\alpha$ .

UIT field 2, near the Bar's center, provides a intriguing instance of what appears to be sequential star formation. A ring of FUV-bright stars with a radius of about 4–5 arcmin ( $\sim 70$ – $90$  pc at a distance of 60 kpc; Hutchings 1982) dominates the field. Figures 2 a) and b) show that the stellar ring is bounded by, and is apparently interacting with, ionized hydrogen in a concentric, larger ring (radius 7–8 arcmin or  $\sim 120$ – $140$  pc). Supernova remnant 0050-728 (Mathewson *et al.* 1984), outlined by the circle in Figure 2b, lies at the northern edge of the shell. HI observations (Staveley-Smith *et al.* 1995, Staveley-Smith *et al.* 1996) show loops comparable in size to the  $H\alpha$  ring near these locations at a range of velocities between about 90 and 130  $\text{km s}^{-1}$ ; the ellipse in Figure 2b shows the location of the ring seen at  $\sim 110$   $\text{km s}^{-1}$ . Fabry-Perot  $H\alpha$  measurements (Okumura 1993)

show linewidths of up to several tens of  $\text{km s}^{-1}$ , reinforcing evidence for ties between the distribution of hot stars and the gas dynamics. In a simple model, the hollow-shell morphology of the HII has been driven by winds from now-defunct hot stars and supernova remnants, which have also propagated star formation from the center outward, as evidenced by relatively gas-free stars in the center of the HII ring. UIT-based detailed analysis of sequential star formation in this region will be the subject of future work (Cornett *et al.* 1996). For example, comparing the distribution of UV-bright stars with that of  $\text{H}\alpha$  emission-line stars and small nebulae as catalogued by (Meyssonier & Azzopardi 1993) will reveal any systematic stellar age gradients in the 0-30 Myr range.

#### 4. Stellar Photometry

Luminosity functions for the four fields, normalized to the number of stars in each for  $14.0 < m(162) < 14.5$ , are shown in Figure 3. From turnovers of the luminosity functions we estimate the limiting FUV magnitudes of the fields to be 14.5, 14.5, 14.5, and 15.0 ( $\pm \sim 0.5$ ) for fields 1-4 respectively, consistent with relative exposure times.

Luminosity functions for fields 1 and 2 show features that may be confirmed from other data. The peak for  $11.0 < m(162) < 11.5$  in field 1’s luminosity function (solid line) is clearly displayed in the field’s color-magnitude diagram as a supergiant “plume” of stars leaving the main sequence (Cornett *et al.* 1994). Field 2 (dashed line) shows a significant overabundance of stars with  $10.0 < m(162) < 11.0$  (more than  $3\sigma$  overabundant compared to each of the other three fields individually) which may be related to sequential star formation in that field. The high-luminosity ends of these  $m(162)$  distributions evidently show structure which reflects recent star formation.

As shown in previous UIT results (*e.g.* J.K.Hill *et al.* 1995) FUV sources are generally well-correlated with  $\text{H}\alpha$  emission. We have compared FUV point-source locations with those of the 711  $\text{H}\alpha$  emission-line stars and small nebulae within the UIT fields of view (Meyssonier & Azzopardi 1993), finding 520 matches at a matching radius of 7.2 arcsec (approximately twice the estimated  $1-\sigma$  the UIT astrometric uncertainty for these images). As described above, a detailed comparison of the spatial distribution of FUV sources with and without associated  $\text{H}\alpha$  emission may provide insights into possible sequential star formation in the SMC.

We have also correlated our stellar photometry tables with the ground-based stellar photometry compiled by Azzopardi & Vigneau (1982; hereafter AV) by positionally matching sources. The precision to which stellar positions are quoted in AV ( $\sim 0.1$  arcmin)

does not permit unambiguous identification of stars fainter than, typically,  $m(162) \sim 15$  because several such stars typically occur in a part of a UIT image of that size. For AV supergiants, this  $m(162)$  limit corresponds to a spectral type of  $\sim F0$ ; therefore, we do not identify or list  $m(162)$  values for AV stars of spectral type F0 or later. (Where available we have used the spectral types listed in AV from Azzopardi 1981 and other sources which employ medium resolution slit spectra as the basis for spectral classification.) Under this spectral type restriction we find 191 sources matched of the 195 within the UIT fields of view. Results of the photometry of these objects are presented in Table 2.

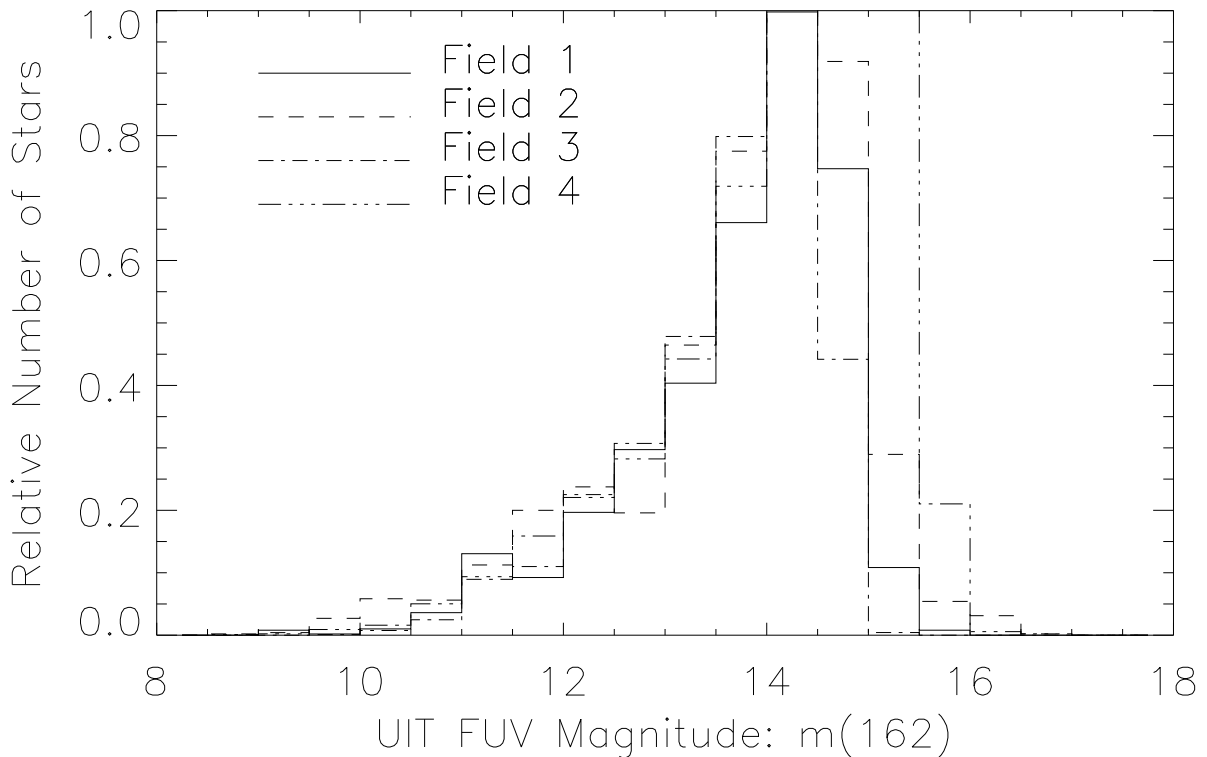


Fig. 3.—  $m(162)$  luminosity functions for the four fields, normalized to the number of stars in each for  $14.0 < m(162) < 14.5$ . The luminosity functions for fields 1 and 2 show features that are confirmed by other data. The peak for  $11.0 < m(162) < 11.5$  in field 1’s luminosity function (solid line) is clearly displayed in the field’s color-magnitude diagram as a supergiant “plume” of stars leaving the main sequence (Cornett *et al.* 1994). In field 2 (dashed line), the overabundance of stars with  $10.0 < m(162) < 11.0$  may be attributable to the effects of sequential star formation in the field.

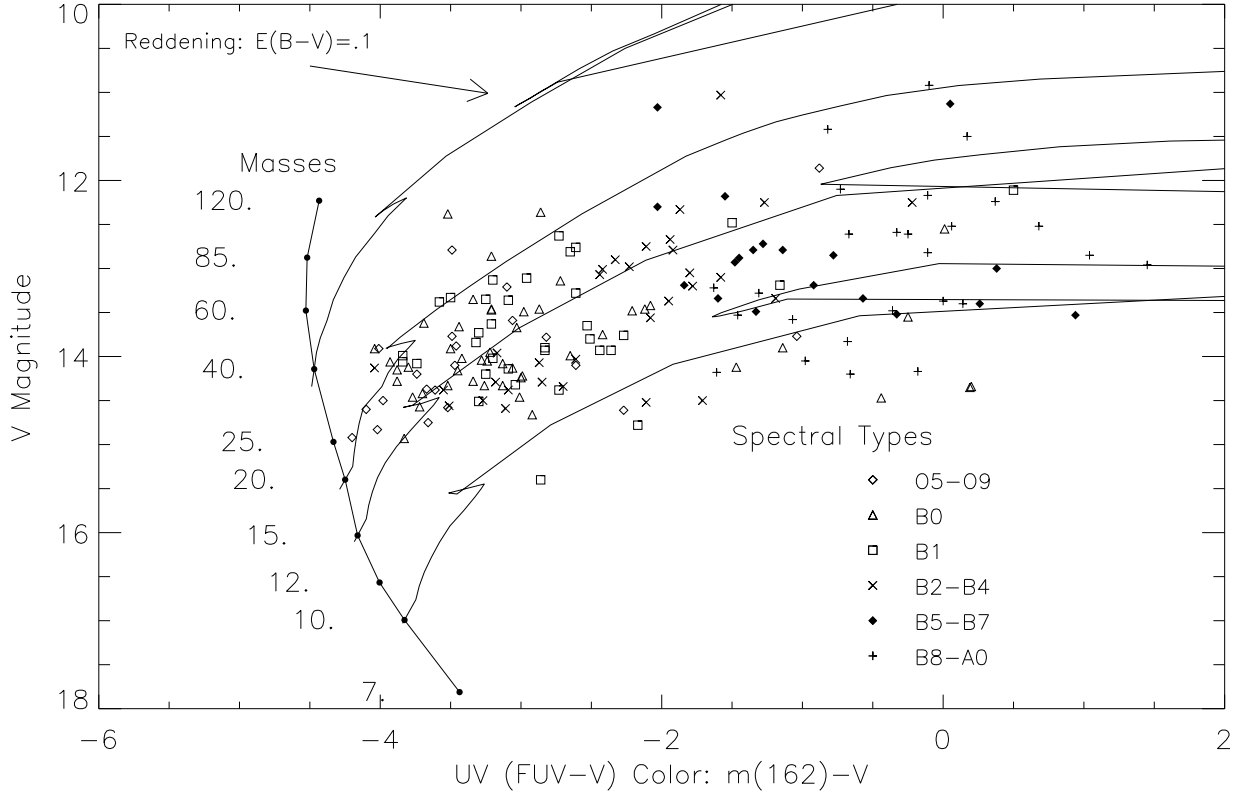


Fig. 4.— The  $(m(162)-V), V$  color-magnitude diagram for 191 stars in common with the catalog of Azzopardi & Vigneau (1982). Discrete symbols are observed stars, with spectral types as noted in the figure. No reddening corrections have been applied to the observed data. The solid lines show SMC-composition stellar models produced by using model atmospheres of Kurucz 1992 on stellar evolution models of Charbonnel *et al.* 1993. Filled circles outline a 1 Myr isochrone, with masses marked; the tracks to the upper right show the subsequent evolutionary paths of 10, 15, 20, and 40  $M_{\odot}$  stars. Model stars are adjusted to distance modulus 18.9 and foreground Galactic extinction  $E(B-V)=0.02$  magnitudes (Hutchings 1982). The reddening vector shown, using the SMC extinction law of Hutchings 1982 and  $E(B-V)=0.1$ , is a typical large value for the SMC (Westerlund 1990). The evolutionary tracks show that these stars predominantly have masses between 10 and 20  $M_{\odot}$  and imply ages between 10 and 30 Myr. The lower limit corresponds to a real absence of supergiant stars brighter than about  $V=11$ . The general segregation of spectral types by color implies that much of the  $(m(162)-V)$  color variation seen in this figure is due to the intrinsic colors of the stars themselves.

Figure 4 is a color-magnitude diagram of the 191 identified stars common to our data and AV, with spectral classes differentiated by different symbols. No reddening corrections have been applied to observed data. SMC-composition stellar models are produced by using model atmospheres of Kurucz 1992 with  $\log(Z/Z_{\odot}) = -0.5$  ( $\sim$ solar/3.2), on stellar evolution models of Charbonnel *et al.* 1993 with  $z = 0.004$  ( $\sim$ solar/5.). These grid points are selected as models with composition parameters nearest to the SMC’s ( $\sim$ solar/4; Westerlund 1990). Filled circles outline a 1 Myr isochrone, with masses marked; the tracks to the upper right show the subsequent evolutionary paths of 10, 15, 20, and 40  $M_{\odot}$  stars. Model stars are adjusted to distance modulus 18.9 and foreground Galactic extinction  $E(B-V)=0.02$  magnitudes (Hutchings 1982). The reddening vector shown, using the SMC extinction curve of Hutchings 1982 and  $E(B-V)=0.1$ , is a typical large value for the SMC (Westerlund 1990). The large FUV/V leverage of extinction in the SMC ( $A_{162}/E(B-V)=15.75$ ) is reflected in the nearly-horizontal orientation of the reddening vector.

The stars catalogued by AV, the visually brightest non-cluster stars in the SMC, are known to be supergiants of a range of spectral types. The evolutionary tracks in Figure 4 clearly demonstrate that these stars predominantly have masses between 10 and 20  $M_{\odot}$ , and therefore, ages between 10 and 30 Myr. The upper age limit is set by the faintness limit of the AV data; however, the lower limit corresponds to a real absence of supergiant stars brighter than about  $V=11$  ( $M\sim 30M_{\odot}$ .) While the effects of some reddening (seen as excesses of  $(m(162)-V)$  color of up to 1.5) are apparent, most color variation seen in this figure is due to the intrinsic color variations of the stars themselves, as seen from the general segregation of spectral types by color.

Figure 5 illustrates the strong variation in  $(FUV-V)$  color with spectral type. The data points are the observed colors, as in Figure 4, plotted against spectral type from AV. The solid line is a spline fit to the observed  $(m(162)-V)$  colors of Galactic supergiants from the atlas of Fanelli *et al.* 1992. The atlas colors have been reddened by the amount of the SMC’s Galactic foreground reddening. The sensitivity of the  $(m(162)-V)$  color to spectral type is evident, as are the significant reddenings for some stars, caused by the large FUV leverage of the SMC extinction law. The atlas colors are seen to form a blue limit for the observed colors, as expected for unreddened stars.

While a true calibration of color *versus* spectral type for SMC stars is not available, Galactic values are probably appropriate for blue stars:  $(m(162)-V)$  colors of Galactic- and SMC-composition model atmospheres differ by less than 0.10 for models that have  $(m(162)-V) < -1.0$ . However, at Galactic  $(m(162)-V)=1.5$ , SMC models are approximately 0.5 mag bluer, with larger differences for redder stars. Therefore, much of the apparent discrepancy between the blue limit of the observed colors and the atlas



colors is probably due to the fact that the locus of colors from an “SMC atlas” would be significantly bluer for stars later than about A0, than the Galactic atlas colors shown.

Figure 5 provides a straightforward method of computing the reddenings along the lines of sight to the stars in AV. We do so by comparing the observed colors to atlas colors for the spectral type, corrected for Galactic foreground reddening, and converting the difference to  $E(B-V)$  using the extinction law of Hutchings 1982. Extinctions computed in this way are presented in Table 2 for all identified AV stars. Stars later in spectral type

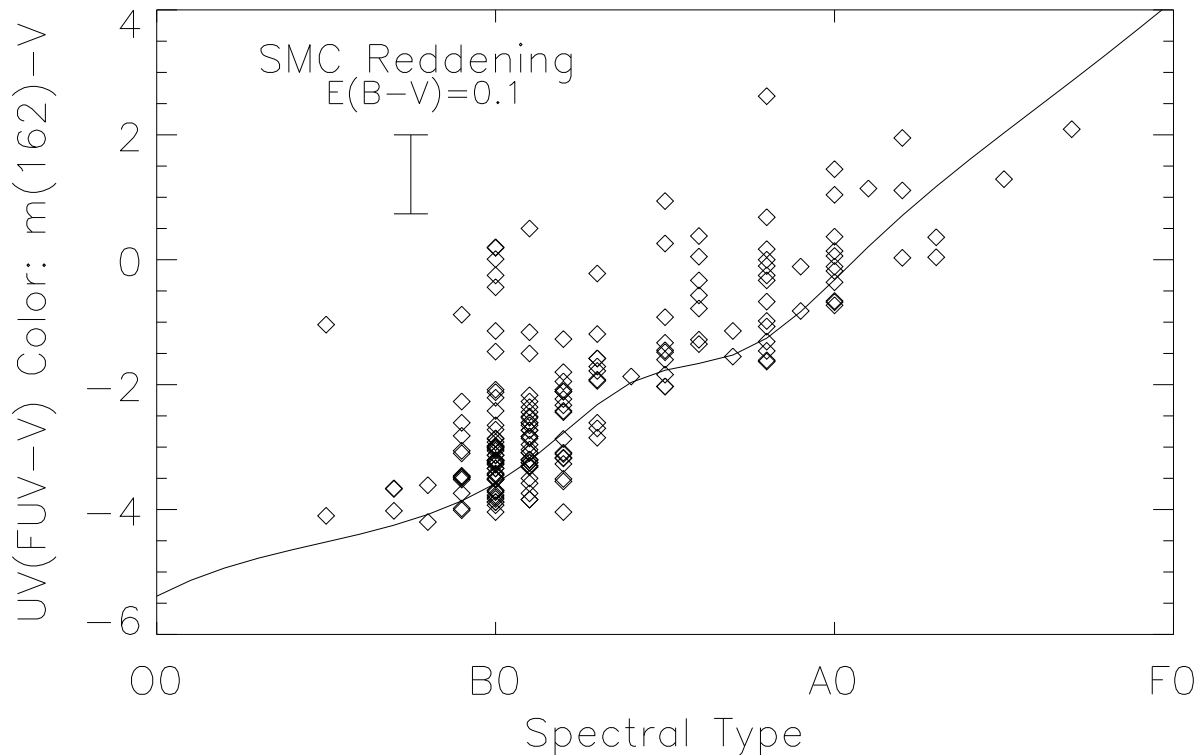


Fig. 5.— *Diamonds*: Stellar spectral type vs  $(m(162)-V)$  color for stars from the catalog of Azzopardi & Vigneau (1982). Where available, spectral types listed in Azzopardi & Vigneau from Azzopardi 1981 and other sources are used, which employ medium resolution slit spectra as the basis for spectral classification. No reddening corrections have been applied to the observed color data. *Solid line*: Spline fit to the  $(m(162)-V)$  colors derived from the spectral atlas of unreddened Galactic stars of Fanelli *et al.* 1992, reddened by  $E(B-V)=0.02$ . Galactic and SMC stellar  $(m(162)-V)$  colors differ by less than 0.10 for stars bluer than  $(m(162)-V)=-1.0$ ; SMC stars are significantly bluer than Galactic stars beyond that limit.

than B8, which have uncertain intrinsic colors, are noted.

Figure 6 shows the resulting  $E(B-V)$  values plotted at the locations of the stars on the SMC, against the  $H\alpha$  image shown in Figure 2a. All values of  $E(B-V) > \sim 0.15$  may be seen from Figure 2b to be at least along the line of sight to  $H\alpha$  emission. The correlation of large reddening values with location implies that these stars are probably associated with the nebulosity.

In the future UIT photometry of the SMC will be supplemented by additional ground-based observations currently underway by the UIT team, as well as by the comprehensive photometric surveys of the Magellanic Clouds (Zaritsky 1996).

## 5. HII Region Photometry

$H\alpha$  emission from HII regions indirectly traces the OB star content of the regions via the process of nebular ionization by the hot stars and subsequent recombination of the hydrogen gas. The FUV continuum emission (*e.g.* at  $1620\text{\AA}$ ) from HII regions arises from OB stars as well as from the more numerous non-ionizing stars (mid-B through early A types.) Therefore, the comparison of  $H\alpha$  and FUV fluxes from HII regions provides a sensitive measure of each HII region’s evolutionary state. Evolutionary models of single-burst ionizing clusters confirm that the ratio of Lyman continuum to FUV flux rapidly decreases with age, with the FUV emission remaining significant for  $\sim 20$  Myr (R.S.Hill *et al.* 1994).

We have measured FUV fluxes for 42  $H\alpha$ -bright HII regions from the catalog of Davies, Elliott, and Meaburn 1976 (hereafter DEM) that were measured at  $H\alpha$  by Kennicutt & Hodge 1986 (hereafter KH), and have compared the observed flux ratios with predictions from cluster models. We compute FUV fluxes in two ways: by summing the flux from stars in the apertures defined by KH; and by summing all flux in pixels in the apertures– the latter method including diffuse FUV emission. (Our use of the KH aperture definitions causes significant aperture overlaps in a few cases.) Table 3 presents fluxes and errors:  $H\alpha$  from KH; FUV from stars (from PSF fits to stars in the aperture); and FUV total fluxes from the apertures themselves.

For the FUV aperture measurements the “sky” flux has been set to zero, and the error term stated does not include a sky contribution. We choose this approximation because the actual sky contribution to any FUV aperture measurement or its uncertainty is very small, and any aperture inside the UIT image area will measure a high background due to SMC material. We set limits on true sky flux by measuring the average background in Astro-2

images made in the UIT B5 filter of a nearby field containing part of the globular cluster 47 Tuc. These images, long exposures (1030 and 1800 sec) made during orbital day, have average earth limb elevation angles and other observational conditions which are typical of those during UIT SMC observations, and therefore give representative background measurements (Waller *et al.* 1995). As measured in this way the sky contribution to the FUV aperture fluxes is  $3.3 \times 10^{-18} \text{erg (cm}^2 \text{\AA s arcsec}^{-2})^{-1}$ , with an average contribution of 0.75% and a maximum of 1.60% to the individual aperture fluxes. These estimates of “sky” contributions are also listed in Table 3.

Figure 7 shows the data from Table 3. Open diamonds are aperture fluxes, and crosses are stellar photometry. No corrections for Galactic foreground reddening have been made to the data. The FUV flux is generally well correlated with its  $H\alpha$  counterpart; furthermore, the ratio of aperture to stellar FUV flux is relatively uniform, especially for brighter HII regions. This ratio measures the relative amounts of bright-star and “diffuse” light, where “diffuse” light here includes contributions from faint stars as well as from dust scattering. The mean value of the ratio of aperture flux to stellar flux, averaged in the log ratio for all HII regions, is 1.79; weighted by flux (the total aperture flux for all HII regions divided by the total stellar flux for all HII regions) is 2.15. Two lines of argument point to a dust-scattering origin for most of the additional FUV flux, however. First, Bohlin *et al.* 1982 have determined the total-to-stellar flux ratio for the Orion nebula, for which the number of undetected stars is small, to be 2.5 for 200-300 $\text{\AA}$  bandpasses near 1400, 1823, 2242, and 2622 $\text{\AA}$ . Second, extrapolating our measured luminosity function for the Field 4, which has the deepest exposure, to  $m(162)=18.0$  (corresponding to an A0 main sequence star, at which spectral type the FUV flux drops rapidly) predicts an additional stellar flux contribution of 22% and a resulting flux-weighted total-to-stellar ratio of 1.76– significantly smaller than the observed value. Scattered-light fractions near the observed SMC value are found in the giant HII regions of M33 (Malumuth *et al.* 1996). Although the small SMC dust abundance (Westerlund 1990) undoubtedly causes the scattering to be significantly less than for Orion, it is nonetheless clear that dust-scattered radiation is a major contributor to the FUV aperture emission from HII regions.

Figure 7 also displays the FUV/ $H\alpha$  ratio, known to be a good diagnostic of HII region evolution (R.S.Hill *et al.* 1994). We have computed  $F(162)/H\alpha$  ratio values for clusters with a single burst of star formation of SMC composition using the IDL procedure CLUSTFLUX (Landsman, personal communication). The ratio rises essentially monotonically from 0.1 at 1 Myr to 4.3 at 10 Myr; ratios for cluster ages of 1Myr, 3Myr, 6.5 Myr, and 8.5 Myr, corrected for foreground Galactic reddening (which increases all  $F(162)/H\alpha$  values by 10%) are plotted as solid lines in Figure 7. For reference, the arrow in Figure 7 shows a typical internal SMC extinction of  $E(B-V)=0.1$ ; Caplan *et al.* 1996 find reddenings local

to SMC bar HII regions in the range  $0.08 < E(B-V) < 0.27$  by comparing 6-cm radio,  $H\alpha$ ,  $H\beta$ , and nearby stellar measurements. Therefore, model and observed ratios agree well for HII-region ages of a few Myr and reasonable internal SMC extinction; the observed HII regions are evidently no older than  $\sim 5$  Myr for any internal SMC reddening, and, for typical assumed SMC reddening, are between 1 Myr and 3 Myr in age. This result is consistent with observations of HII regions in galaxies as disparate as NGC 4449 (R.S.Hill

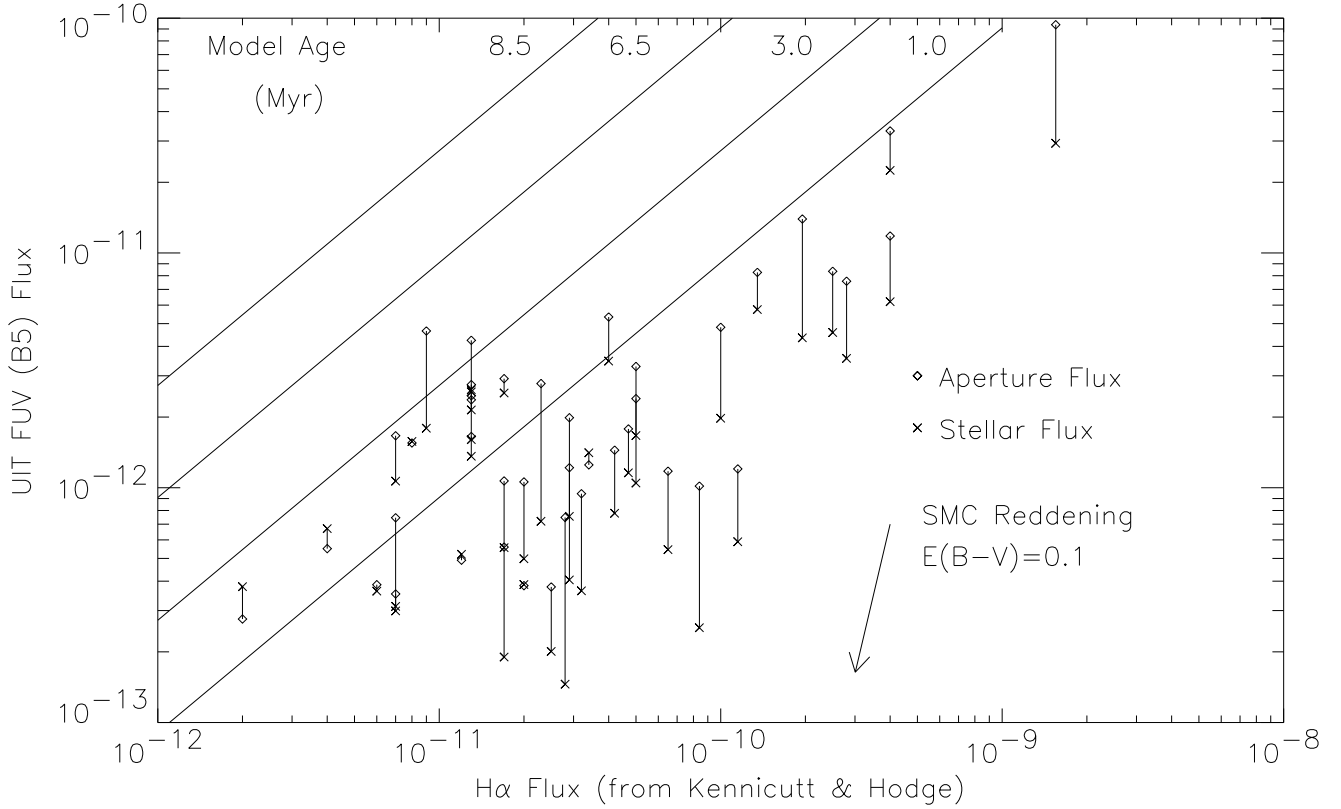


Fig. 7.— FUV ( $\lambda_{eff} = 1620\text{\AA}$ ) vs  $H\alpha$  flux for HII regions as defined by the apertures of Kennicutt & Hodge (1986). *Crosses* mark the total FUV stellar flux, from our stellar photometry, of stars which lie within the KH apertures. *Diamonds* mark the total FUV flux contained within the apertures. No reddening corrections are applied to the data, although a typical SMC internal reddening corresponding to  $E(B-V)=0.1$  is shown. *Solid lines* at constant FUV/ $H\alpha$  mark the expected FUV/ $H\alpha$  ratios for clusters of single-burst formation of stars of SMC composition, reddened to Galactic foreground values. The ages of the clusters are 1 Myr, 3 Myr, 6.5 Myr, and 8.5 Myr respectively, with the smallest FUV/ $H\alpha$  value corresponding to age 1 Myr.

*et al.* 1994) and M81 (J.K.Hill *et al.* 1995). There is also a clear tendency for H $\alpha$ -bright HII regions to be either relatively young– which is not surprising– or unreddened. The absence of significantly older HII regions is most likely a selection effect originating in KH’s bias for H $\alpha$ -bright HII regions.

## 6. Summary

UIT FUV images and derived stellar photometry for most of the Bar of the SMC are presented. The UV morphology of the SMC’s Bar shows four concentrations of UV-bright stars spread from northeast to southwest at nearly equal ( $\sim 30$  arcmin) spacings. One of the concentrations, near DEM 55, appears as a well-defined 8-arcmin diameter ring surrounded by a larger H $\alpha$  ring and strongly suggests sequential star formation.

FUV PSF photometry, resulting in  $m(162)$  magnitudes, is obtained for 11,306 stars. We present a FUV luminosity function for the SMC bar, complete to  $m(162) \sim 14.5$ , and compare our photometry with the compiled ground-based data of AV. Detected objects are well correlated with other SMC Population I material; 520 of 711 H $\alpha$  emission-line stars and small nebulae within the UIT fields of view are identified with FUV sources. For early type stars, the bluest observed ( $m(162)$ –V) colors for each spectral type agree well with values computed from unreddened Galactic spectral atlas stars for types earlier than about A0; for later types, observed SMC stars range significantly bluer, as predicted by low-metallicity models. We attribute redder colors for some stars of all spectral types to strong FUV extinction due to even small amounts of SMC dust. Internal SMC reddenings are determined for all catalog stars. All stars with  $E(B-V) > 0.15$  are within regions of visible H $\alpha$  emission.

FUV photometry is obtained for the resolved stars and for the total emission from DEM HII regions in the SMC Bar. The flux-weighted ratio of total to stellar flux for DEM HII regions using the apertures of KH is 2.15; since only 22% more flux is contributed by stars fainter than  $m(162)=14.5$ , most of the excess total flux is due to scattered FUV from dust. Stellar and total emission from DEM HII regions are well correlated with H $\alpha$  fluxes measured by KH. We compute ratios of FUV to H $\alpha$  flux for 42 SMC HII regions and compare them with model results, finding that the observed ratios for all H $\alpha$ -selected HII regions are consistent with models of SMC metallicity, ages from 1-5 Myr, and moderate ( $E(B-V)=0.0-0.1$  mag) extinction.

We gratefully acknowledge the contributions made by the many people involved in the *Astro-2* mission. We thank Robert S. Hill, Wayne Landsman, and Michael Fanelli for useful

discussions, Greg Bothun for the use of his H $\alpha$  image of the SMC, Joel Offenberg for help in preparing publication-quality images, and Joan Hollis and Emily Zamkoff for data entry and programming assistance. We also thank Lister Staveley-Smith for kindly supplying a digital version of a part of his HI maps of the complete SMC.

Funding for the UIT project has been through the Spacelab Office at NASA under project number 440-51. RWO gratefully acknowledges NASA support of portions of this research through grants NAG5-700 and NAGW-2596 to the University of Virginia.

## REFERENCES

- Azzopardi, M. 1981, Ph.D. Thesis, Paul Sabatier University of Toulouse, No. 979.
- Azzopardi, M. & Vigneau, J. 1982, A&AS 50, 291.
- Bohlin, R.C., Hill, J.K., Stecher, T.P., and Witt, A.N. 1982, ApJ 255, 87.
- Bothun, G. (personal communication).
- Caplan, J., Ye, T., Deharveng, L., Turtle, A., and Kennicutt, R. 1996, A&A 307, 403.
- Charbonnel, C., Meynet, G., Maeder, A., Schaller, G., & Schaerer, D. 1993, A&AS 101, 415.
- Cornett, R.H., Hill, J.K., Bohlin, R.C., O’Connell, R.W., Roberts, M.S., Smith, A.M., & Stecher, T.P. 1994, ApJ 425, L117.
- Cornett *et al.* 1996, in preparation.
- Davies, R.D., Elliott, K.H., and Meaburn, J. 1976, MmRAS 81, 89.
- Fanelli, M.N., O’Connell, R.W., Burstein, D. & Wu, C.-C. 1992, ApJS 82, 197.
- Hill, J.K., Bohlin, R.C., Cheng, K-P., Fanelli, M.N., Hintzen, P.M.N., O’Connell, R.W., Roberts, M.S., Smith, A.M., Smith, E.P., & Stecher, T.P. 1993, ApJ 413, 610.
- Hill, J.K., Cheng, K-P., Bohlin, R.C., Cornett, R.H., Hintzen, P.M.N., O’Connell, R.W., Roberts, M.S., Smith, A.M., Smith, E.P., & Stecher, T.P. 1995, ApJ 438, 182.
- Hill, R.S., Home, A.T., Smith, A.M., Bruhweiler, F.C., Cheng, K.-P., Hintzen, P.M., and Oliverson, R.J. 1994, ApJ 430, 568.
- Hutchings, J.B. 1982, ApJ 255, 70.

- Kennicutt, R.C. Jr. & Hodge, P.W. 1986, ApJ 306,130.
- Kurucz, R.L. 1992, in *The Stellar Populations of Galaxies*, ed. B. Barbuy & A. Renzini (Dordrecht: Kluwer Academic), 225.
- Landsman, W.B. (personal communication).
- Lasker, B.M., Sturch, C.R., McLean, B.J., Russell, J.L., Jenkner, H. & Shara, M.M. 1989, Space Telescope Science Institute Preprint No. 363.
- Malumuth, E.M., Waller, W.H., and Parker, J. Wm. 1996, AJ 111, 1128.
- Mathewson, D.S., Ford, V.L., Dopita, M.A., Tuohy, I.R., Mills, B.Y., & Turtle, A.J. 1984, ApJS 55, 189.
- Meyssonier, N. and Azzopardi, M. 1993, A&AS 102, 451.
- Okumura, K., 1993, Ph.D. dissertation, University of Paris.
- Parker, J. Wm. 1996, in preparation.
- Smith, A.M., Cornett, R.H., and Hill, R.S. 1987, ApJ 320, 609.
- Staveley-Smith, L., Sault, R.J., McConnell, D., Kesteven, M.J., Hatzidimitriou, D., Freeman, K.C., and Dopita, M.A. 1995, *Pub. Astr. Soc. Austr.* 12, 13.
- Staveley-Smith, L., Sault, R.J., Hatzidimitriou, D., Kesteven, M.J., & McConnell, D. 1996, MNRAS in press.
- Stecher *et al.* 1992, ApJ 395, L1.
- Stecher *et al.* 1996, submitted to PASP.
- Stetson, P.B. 1987, PASP 99, 101.
- Waller, W.H., Marsh, M., Bohlin, R.C., Cornett, R.H., Dixon, W.V., Isensee, J.E., Murthy, J., O’Connell, R.W., Roberts, M.S., Smith, A.M., & Stecher, T.P. 1995 AJ 110, 1255.
- Westerlund, B.E. 1990 A&A Rev. 2,29.
- Zaritsky, D.L. 1996, in preparation.

Fig. 1.— A far-UV (FUV) mosaic of the Small Magellanic Cloud. It is made up of the longest FUV ( $\lambda_{eff} = 1620\text{\AA}$ ) exposures of SMC fields made by UIT during the Astro-1 and Astro-2 missions. Exposure times range from 117 to 898 seconds; see Table 1 for observational details. The bright clusters centered in Fields 4 and 3 respectively are NGC 346 and NGC 330; the field of view shown encompasses nearly the entire SMC bar, and the resolution is  $\sim 3''$ .

Fig. 2.— a) The SMC H $\alpha$  "parking lot camera" image obtained by Bothun (personal communication) displayed on a linear greyscale. —b) Linearly spaced contours from Figure 2a) superimposed on the image of Figure 1. A constant background has been subtracted. Note the prominent ring of H $\alpha$  emission surrounding, and larger than, the ring of FUV-bright stars in Field 2. SNR 0050-728 (Mathewson *et al.* 1984) is marked in size and position by the circle at the northern edge of the ring. A prominent ring of HI emission, seen over a range of radial velocities centered at  $\sim 110\text{km s}^{-1}$  in the data of Staveley-Smith *et al.* 1995, is outlined by the ellipse.

Fig. 6.— Stellar reddening ( $E(B-V)$ ) map, computed by comparing the observed ( $m(162)-V$ ) colors for stars from the catalog of Azzopardi & Vigneau (1982) with the Galactic atlas spline fit for that spectral type shown in Figure 5. Stellar symbol diameter is proportional to  $E(B-V)$  as shown in the legend. Observed colors have been corrected for Galactic foreground reddening. All values of  $E(B-V) > \sim 0.15$  may be seen from Figure 2b to be at least along the line of sight to H $\alpha$  emission. The correlation of large reddening values with location implies that these stars are probably associated with the nebulosity.



TABLE 1. Observational parameters for UIT images of the Small Magellanic Cloud.

TABLE 2. Observational data for stars from Azzopardi & Vigneanu 1982 (AV) which were observed by UIT. AV stars which are within UIT fields but later in spectral type than A9 are omitted, since they are too faint in the FUV for detection by UIT.  $m(162)$  values are derived from PSF photometry as described in the text.  $E(B-V)$  values are derived by comparing the unreddened  $(m(162)-V)$  color for the stellar spectral type with the observed color, using the reddening law of Hutchings 1982.

TABLE 3. Fluxes for HII regions from the list of Davies, Elliott, & Meaburn 1976 (DEM) as measured by Kennicutt & Hodge 1986 (KH) which are completely contained within the UIT field of view. “FUV Stellar” flux is the total flux of stars within the aperture defined by KH; “FUV Aperture” flux is the total pixel flux contained within the aperture defined by KH; and “Sky Flux” is an estimate for the non-SMC sky contribution within the aperture, as described in the text.

Table 1. UIT FUV Images of the SMC

Field	Field Center RA (2000.0) Dec	Exposure Times (sec)	Obs. Epoch (GMT)	No. Stars	Flight
1	00 47 33.7 -73 06 26.8	23.9,117.0	12/05/90 06:16	1713	Astro-1
2	00 50 58.3 -72 44 56.5	25.9,247.0	03/16/95 23:50	2110	Astro-2
3	00 56 41.2 -72 28 28.8	18.7,459.0	03/06/95 06:14	2517	Astro-2
4	00 59 24.2 -72 11 08.4	36.2,179.0,898.	03/09/95 04:04	4966	Astro-2

Table 2. UIT FUV Magnitudes of AV Stars

#	AV #	UIT #	R.A. (2000.0) Dec (Azzopardi and Vigneau)	Sp	V	UIT m(162)	$\sigma$	E(B-V)
1	2B	1686	00 43 51.2 -73 08 54	B0	13.49	10.51	0.10	0.05
2	3	70	00 44 29.6 -72 58 00	B0	14.12	12.65	0.07	0.17
3	6	1699	00 45 19.8 -73 15 18	B0	13.46	10.25	0.08	0.03
4	7	1417	00 45 33.7 -73 04 31	B0	14.57	10.85	0.06	-0.01
5	8	1505	00 45 36.2 -72 59 12	B8	13.53	12.07	0.05	-0.02
6	9	1694	00 45 37.1 -73 14 07	B2	13.05	11.25	0.07	0.08
7	11	1622	00 45 54.3 -73 16 13	B2	13.56	11.48	0.05	0.05
8	12	1429	00 46 2.8 -73 06 19	O9	13.21	10.11	0.07	0.06
9	14	321	00 46 33.2 -73 05 55	O5	13.77	12.73	0.07	0.28
10	16	1558	00 46 55.8 -73 08 25	B1	13.19	12.03	0.10	0.16
11	17	1522	00 47 3.6 -73 05 55	B1	13.76	11.49	0.12	0.08
12	17A	1679	00 47 4.8 -73 06 19	B2	13.37	11.42	0.10	0.07
13	18	1433	00 47 13.1 -73 06 25	B1	12.48	10.98	0.04	0.14
14	19	2766	00 47 15.8 -72 49 55	B6	13.00	13.38	0.08	0.16
15	20	158	00 47 29.9 -73 01 25	B8:	12.14	14.76	0.08	0.31
16	21	1690	00 47 32.6 -73 10 56	B1	14.14	11.05	0.05	0.01
17	22	1444	00 47 39.8 -73 07 38	B2	12.25	10.98	0.06	0.12
18	23	1670	00 47 40.1 -73 22 43	B3	12.25	12.03	0.08	0.17
19	24	1675	00 47 42.9 -73 02 25	O9	13.78	10.96	0.07	0.08
20	25	1597	00 47 47.5 -73 12 19	B5	13.19	11.35	0.10	-0.01
21	26	514	00 47 50.5 -73 08 14	B0	12.55	12.56	0.07	0.28
22	27	947	00 47 51.6 -73 14 14	A2	12.17	14.12	0.05	0.10 <sup>c</sup>
23	28	1662	00 47 55.0 -73 21 14	B0	13.42	11.34	0.08	0.12
24	31	361	00 48 7.2 -73 06 32	B8:	12.52	13.20	0.06	0.15
25	32	1939	00 48 10.2 -72 43 44	B1	14.20	10.95	0.03	0.00
26	34	-1	00 48 18.7 -73 23 38	B2:	13.81	0.00	0.00	-9.99 <sup>b</sup>
27	35	-1	00 48 21.3 -72 51 02	B0:	14.13	0.00	0.00	-9.99 <sup>a</sup>
28	36	1934	00 48 23.9 -72 43 38	B1	14.02	10.82	0.04	0.00
29	37	1676	00 48 27.0 -73 03 20	B5	12.88	11.43	0.07	0.03
30	38	142	00 48 28.2 -73 00 32	A0	12.85	13.89	0.05	0.11 <sup>c</sup>
31	39A	1476	00 48 31.4 -73 15 32	W6	99.99	10.94	0.06	-9.99 <sup>d</sup>
32	41	1767	00 48 36.1 -72 52 50	B2	14.56	11.05	0.06	-0.06
33	42	2265	00 48 40.2 -72 58 14	B5	13.49	12.16	0.09	0.03
34	43	1875	00 48 48.8 -72 46 14	B1	14.08	10.34	0.04	-0.04

Table 2—Continued

#	AV #	UIT #	R.A. (2000.0) Dec (Azzopardi and Vigneau)	Sp	V	UIT m(162)	$\sigma$	E(B-V)
35	45	-1	00 48 50.3 -73 22 02	B8	14.15	0.00	0.00	-9.99 <sup>a</sup>
36	48	1709	00 49 3.4 -73 21 32	B3	11.03	9.45	0.12	0.06
37	50	1765	00 49 16.7 -72 52 32	B1	13.11	10.15	0.05	0.02
38	51	1777	00 49 32.8 -72 51 08	B0	14.05	10.81	0.03	0.03
39	53	2495	00 49 45.8 -72 52 38	A0	12.96	14.41	0.05	0.14 <sup>c</sup>
40	55	1197	00 49 48.2 -73 17 45	B5	13.40	13.66	0.06	0.16
41	56	1751	00 49 51.7 -72 55 39	B5	11.17	9.14	0.04	-0.02
42	58	1769	00 49 58.3 -72 51 45	B2	14.38	10.83	0.04	-0.06
43	59	788	00 49 58.4 -73 11 33	A0	13.40	13.54	0.06	0.04 <sup>c</sup>
44	62	2361	00 50 1.2 -72 55 03	B3	14.34	11.64	0.03	-0.03
45	63	672	00 50 0.9 -73 10 08	A0	13.48	13.12	0.06	0.00 <sup>c</sup>
46	65	1448	00 50 6.9 -73 07 39	B6	11.13	11.18	0.08	0.14
47	66	1642	00 50 6.7 -73 16 21	B0	13.48	11.27	0.09	0.11
48	67	2039	00 50 11.9 -72 32 27	B0	13.66	10.22	0.07	0.01
49	69	2442	00 50 18.0 -72 53 21	B0	13.35	10.01	0.21	0.02
50	70	2007	00 50 18.9 -72 38 03	B0	12.38	8.86	0.04	0.00
51	73	1677	00 50 28.4 -73 03 09	B0	14.08	10.95	0.07	0.04
52	75	1757	00 50 32.9 -72 52 27	O9	12.79	9.30	0.04	0.03
53	77	1827	00 50 34.2 -72 47 39	B0	13.91	10.41	0.03	0.01
54	80	1824	00 50 44.3 -72 47 33	B1	13.33	9.83	0.04	-0.02
55	82	1925	00 50 49.8 -72 42 33	B2	14.13	10.09	0.06	-0.10
56	83	1930	00 50 52.8 -72 42 03	B1	13.38	9.80	0.04	-0.03
57	85	2440	00 51 0.8 -72 52 57	B0	13.75	11.33	0.05	0.09
58	87	3400	00 51 8.3 -72 40 03	B0	13.90	12.76	0.11	0.19
59	89	1121	00 51 10.4 -73 15 45	B0	14.47	14.03	0.09	0.25
60	90	-1	00 51 12.1 -72 28 09	A5	12.58	0.00	0.00	-9.99 <sup>a</sup>
61	91	2325	00 51 11.5 -72 55 09	B8	12.61	12.36	0.04	0.08
62	93	1940	00 51 20.8 -72 41 21	B0:	14.13	11.07	0.06	0.04
63	94	1783	00 51 20.6 -72 49 33	B1	13.99	10.15	0.04	-0.05
64	95	1885	00 51 21.9 -72 44 03	O9	13.91	9.90	0.04	-0.01
65	99	1809	00 51 25.4 -72 47 45	B2	13.01	10.59	0.04	0.03
66	100	1743	00 51 26.9 -72 57 45	B3	14.29	11.44	0.05	-0.04
67	102	2036	00 51 36.5 -72 32 09	B2	14.29	11.11	0.07	-0.03
68	103	1847	00 51 36.7 -72 45 57	B1	13.36	10.27	0.03	0.01

Table 2—Continued

#	AV #	UIT #	R.A. (2000.0) Dec (Azzopardi and Vigneau)	Sp	V	UIT m(162)	$\sigma$	E(B-V)
69	104	1800	00 51 39.0 -72 47 57	B1	13.13	9.93	0.04	0.00
70	105	3885	00 51 41.9 -72 27 57	A0	12.24	12.61	0.07	0.05 <sup>c</sup>
71	106	2005	00 51 44.1 -72 37 15	B1	14.32	11.28	0.05	0.01
72	109	1976	00 51 50.6 -72 39 15	B1	13.73	10.43	0.03	-0.01
73	110	1877	00 51 52.8 -72 44 03	A0	12.17	12.06	0.06	0.02 <sup>c</sup>
74	111	2035	00 51 56.7 -72 31 57	B1	13.84	10.52	0.06	-0.01
75	112	2031	00 51 58.5 -72 33 15	B0	14.15	10.27	0.05	-0.02
76	114	1971	00 52 3.1 -72 39 22	B0	14.93	11.10	0.05	-0.02
77	122	1932	00 52 25.7 -72 40 52	B6	12.79	11.44	0.05	0.02
78	123	1758	00 52 27.8 -72 50 58	B8	13.22	11.59	0.06	-0.03
79	126	1961	00 52 31.7 -72 39 22	B0	13.47	10.26	0.04	0.03
80	131	1841	00 52 41.0 -72 45 10	B8	12.61	11.94	0.07	0.05
81	133	2003	00 52 44.2 -72 36 46	B0	13.91	9.87	0.04	-0.04
82	137	1865	00 52 53.0 -72 44 04	B4	12.33	10.46	0.04	0.01
83	138	1784	00 52 52.9 -72 48 22	B0	14.28	10.94	0.05	0.02
84	141	3723	00 53 10.5 -72 33 40	B3:	14.50	12.79	0.04	0.05
85	143	1970	00 53 27.1 -72 38 22	B0	14.12	10.32	0.04	-0.02
86	144	1742	00 53 33.7 -72 56 16	B0	14.06	10.13	0.08	-0.03
87	145	1983	00 53 36.0 -72 37 40	B1	13.35	10.10	0.05	0.00
88	148	1882	00 53 42.5 -72 42 28	B0	14.28	10.40	0.04	-0.02
89	149	1774	00 53 53.6 -72 48 22	B2	13.96	10.79	0.07	-0.03
90	150	4034	00 53 58.3 -72 28 35	B6	12.72	11.44	0.05	0.03
91	151	1807	00 53 59.6 -72 45 53	B5	12.30	10.27	0.06	-0.02
92	152	5913	00 54 4.2 -72 31 40	A3	11.87	12.23	0.03	-0.06 <sup>c</sup>
93	153	3451	00 54 4.0 -72 37 17	B8	13.58	12.51	0.06	0.01
94	154	3095	00 54 9.9 -72 41 34	B0:	13.55	13.30	0.05	0.26
95	155	2975	00 54 15.2 -72 42 59	B0:	14.34	14.54	0.10	0.30
96	156	4384	00 54 19.4 -72 17 47	A0	14.17	13.99	0.06	0.01 <sup>c</sup>
97	157	3938	00 54 23.0 -72 17 05	B0	14.33	11.07	0.05	0.03
98	158	3946	00 54 23.5 -72 18 59	B1	14.06	10.22	0.04	-0.05
99	160	2340	00 54 43.5 -72 51 53	B0	13.99	11.34	0.07	0.07
100	164	4070	00 55 16.0 -72 41 17	B0	14.16	10.71	0.04	0.01
101	165	3994	00 55 19.9 -72 25 59	B7	12.79	11.65	0.06	0.03
102	169	4077	00 55 40.3 -72 44 54	B1	13.90	11.07	0.05	0.03

Table 2—Continued

#	AV #	UIT #	R.A. (2000.0) Dec (Azzopardi and Vigneau)	Sp	V	UIT m(162)	$\sigma$	E(B-V)
103	171	6141	00 55 48.2 -72 39 23	B6	13.34	12.77	0.05	0.09
104	172	10309	00 55 54.9 -72 08 54	B8	13.37	13.37	0.06	0.10
105	174	8802	00 56 38.6 -72 01 36	A7	12.43	14.52	0.07	-0.06 <sup>c</sup>
106	175	4036	00 56 38.9 -72 36 30	B1	13.65	11.12	0.05	0.05
107	176	3947	00 56 39.7 -72 25 06	B1	13.93	11.10	0.04	0.03
108	177	6454	00 56 45.1 -72 03 30	O5	14.60	10.50	0.03	0.03
109	178	3970	00 56 48.6 -72 28 42	B2	14.38	11.29	0.06	-0.03
110	180	7161	00 56 55.8 -72 24 12	B5	13.19	12.27	0.09	0.07
111	181	11001	00 56 57.8 -72 17 36	A0	13.83	13.15	0.04	-0.03 <sup>c</sup>
112	182	6480	00 57 1.6 -72 08 06	B0	14.33	10.81	0.03	0.00
113	184	7143	00 57 14.4 -72 22 24	B8	14.18	12.57	0.07	-0.03
114	185	6777	00 57 24.4 -72 01 30	B8:	13.28	11.97	0.06	0.00
115	186	4000	00 57 27.8 -72 33 06	O9	14.10	10.63	0.05	0.03
116	189	3958	00 57 33.3 -72 28 48	B1	14.51	11.21	0.05	-0.01
117	190	11396	00 57 35.1 -72 26 48	B6	13.52	13.19	0.08	0.11
118	191	6482	00 57 37.8 -72 13 00	B1	13.63	10.42	0.06	0.00
119	192	6490	00 57 38.2 -72 21 49	O9	14.58	11.06	0.05	0.03
120	193	7152	00 57 38.1 -72 24 31	B1	15.40	12.54	0.09	0.03
121	194	4008	00 57 45.6 -72 35 30	B0	13.95	10.73	0.04	0.03
122	195	5818	00 57 45.5 -72 40 12	B5	13.53	14.47	0.04	0.21
123	196	7163	00 57 54.7 -72 27 37	B1	13.93	11.57	0.09	0.07
124	199	5274	00 58 2.3 -72 35 37	A3	13.41	13.45	0.03	-0.09 <sup>c</sup>
125	200	4025	00 58 8.1 -72 38 25	A0	12.10	11.37	0.05	-0.03 <sup>c</sup>
126	201	6479	00 58 10.7 -72 10 55	B0	14.04	10.76	0.06	0.02
127	202	6855	00 58 15.5 -72 07 25	B0	14.33	11.20	0.05	0.04
128	204	3998	00 58 22.5 -72 35 13	B1:	14.38	11.65	0.05	0.04
129	205	11006	00 58 23.5 -72 21 31	A2	12.30	13.41	0.04	0.03 <sup>c</sup>
130	207	6429	00 58 33.7 -71 55 43	O7	14.37	10.70	0.06	0.05
131	208	5549	00 58 33.7 -72 39 25	O9	14.10	11.49	0.10	0.10
132	209	7135	00 58 35.9 -72 24 55	B0	14.46	11.45	0.04	0.05
133	210	6484	00 58 36.7 -72 16 19	B3	12.67	10.73	0.05	0.03
134	211	7145	00 58 41.8 -72 26 13	B8	11.50	11.67	0.07	0.11
135	213	6607	00 58 55.1 -71 56 31	A2	12.11	12.14	0.08	-0.05 <sup>c</sup>
136	214	6964	00 58 55.2 -72 13 13	B3	13.34	12.15	0.03	0.09

Table 2—Continued

#	AV #	UIT #	R.A. (2000.0) Dec (Azzopardi and Vigneau)	Sp	V	UIT m(162)	$\sigma$	E(B-V)
137	215	3955	00 58 55.9 -72 32 01	B1	12.76	10.15	0.06	0.05
138	217	7050	00 59 2.3 -72 18 49	B2:	14.59	11.48	0.03	-0.03
139	218	7064	00 59 5.2 -72 19 37	B1	13.80	11.29	0.05	0.06
140	219	7010	00 59 7.7 -72 16 31	B2:	14.50	11.23	0.06	-0.04
141	220	6446	00 59 10.9 -72 05 43	O9	14.50	10.52	0.06	-0.01
142	221	3945	00 59 10.2 -72 31 31	B0	13.46	11.34	0.05	0.12
143	222	7080	00 59 13.5 -72 20 55	B3	13.20	11.42	0.06	0.04
144	223	4007	00 59 13.6 -72 38 55	B0	13.67	10.64	0.02	0.04
145	224	6732	00 59 16.9 -72 04 37	B0	14.22	11.23	0.05	0.05
146	225	4313	00 59 16.8 -72 29 43	B8	14.05	13.07	0.03	0.02
147	226	6481	00 59 21.4 -72 17 07	B0	14.42	10.72	0.05	-0.01
148	229	8932	00 59 27.5 -72 09 49	O9	11.86	10.98	0.16	0.24
149	230	6435	00 59 30.1 -72 01 02	B2	12.75	10.64	0.05	0.05
150	231	10562	00 59 29.6 -72 20 14	A0	14.20	13.54	0.04	-0.03 <sup>c</sup>
151	232	-1	00 59 32.9 -72 10 43	O9	12.36	0.00	0.00	-9.99 <sup>e</sup>
152	234	6440	00 59 44.3 -72 04 13	B2	12.98	10.75	0.04	0.04
153	237	7019	00 59 53.5 -72 19 02	B8	12.59	12.26	0.03	0.07
154	238	6475	00 59 56.0 -72 13 32	O9	13.77	10.28	0.06	0.03
155	240	3921	01 00 1.1 -72 23 50	B3	14.03	11.42	0.05	-0.02
156	242	9303	01 00 7.9 -72 13 56	B1	12.11	12.61	0.07	0.29
157	245	6543	01 00 16.7 -71 57 02	B5	13.34	11.74	0.06	0.01
158	250	6589	01 00 23.8 -71 59 26	B9	12.82	12.71	0.08	0.06 <sup>c</sup>
159	251	3932	01 00 22.9 -72 30 44	O7	14.75	11.09	0.06	0.05
160	252	6450	01 00 30.6 -72 10 56	B2:	13.07	10.63	0.05	0.03
161	257	6486	01 00 45.1 -72 23 50	B3	12.79	10.87	0.05	0.03
162	260	6453	01 00 52.0 -72 13 32	B1	13.28	10.67	0.05	0.05
163	263	6813	01 01 6.9 -72 12 57	B6	12.85	12.07	0.04	0.07
164	264	6422	01 01 8.4 -71 59 56	B0	12.36	9.50	0.12	0.06
165	266	6489	01 01 10.1 -72 27 26	B1	12.63	9.90	0.06	0.04
166	267	6439	01 01 16.0 -72 06 32	O8	14.92	10.72	0.03	-0.01
167	268	6448	01 01 16.4 -72 12 39	B0:	13.14	10.42	0.06	0.07
168	270	6477	01 01 17.5 -72 17 27	B9	11.42	10.60	0.05	0.00 <sup>c</sup>
169	271	6476	01 01 20.5 -72 17 15	B0	13.46	10.59	0.06	0.06
170	272	9881	01 01 23.4 -72 20 09	B2	14.52	12.41	0.05	0.05

Table 2—Continued

#	AV #	UIT #	R.A. (2000.0) Dec (Azzopardi and Vigneau)	Sp	V	UIT m(162)	$\sigma$	E(B-V)
171	273	7855	01 01 27.9 -72 07 03	A1	12.18	13.32	0.04	0.07 <sup>c</sup>
172	274	6483	01 01 29.8 -72 23 15	B0	14.02	10.60	0.06	0.01
173	277	6824	01 01 33.0 -72 14 39	B2	14.07	11.20	0.05	-0.01
174	279	6428	01 01 35.2 -72 03 03	O9	14.20	10.46	0.04	0.01
175	280	6580	01 01 39.9 -72 02 27	B0	14.66	11.74	0.05	0.05
176	282	6447	01 01 50.4 -72 13 09	O7	14.83	10.81	0.04	0.02
177	286	6605	01 01 57.8 -72 04 15	A5	12.35	13.64	0.07	-0.06 <sup>c</sup>
178	287	6444	01 01 57.5 -72 12 39	B0	12.86	9.65	0.05	0.03
179	290	6561	01 02 0.8 -72 02 21	B1	13.93	11.49	0.07	0.06
180	291	6816	01 02 4.6 -72 15 27	B1	14.78	12.61	0.04	0.08
181	292	6923	01 02 4.5 -72 19 03	B3	13.10	11.52	0.05	0.06
182	296	6445	01 02 8.8 -72 13 15	O8	14.38	10.77	0.03	0.04
183	297	6419	01 02 10.4 -72 00 21	B7	12.18	10.63	0.06	0.00
184	298	6560	01 02 12.7 -72 02 51	A0	12.52	12.58	0.09	0.03 <sup>c</sup>
185	299	6980	01 02 13.9 -72 22 09	O9	14.61	12.34	0.07	0.13
186	300	6442	01 02 14.8 -72 11 15	B0	14.46	10.69	0.05	-0.01
187	301	6512	01 02 15.7 -71 59 45	B0	14.24	11.24	0.08	0.05
188	302	9841	01 02 19.3 -72 22 03	B0	14.35	14.54	0.11	0.30
189	303	6418	01 02 22.3 -72 00 15	B1	12.81	10.16	0.07	0.05
190	312	6441	01 02 45.8 -72 12 03	B0	13.62	9.93	0.02	-0.01
191	314	8760	01 02 48.6 -72 16 39	B2	12.90	10.57	0.12	0.04
192	315	6438	01 02 50.0 -72 10 09	B8	10.92	10.82	0.07	0.09
193	318	6436	01 02 54.8 -72 09 51	O9	13.59	10.53	0.05	0.06
194	321	6433	01 02 57.8 -72 08 03	O9	13.88	10.42	0.06	0.03

<sup>a</sup>No detection by UIT; within 3 arcmin of field edge.

<sup>b</sup>No detection by UIT; m(162)>14.5.

<sup>c</sup>Spectral type later than B8; intrinsic color and E(B–V) therefore uncertain.

<sup>d</sup>No magnitude supplied by AV.

<sup>e</sup>Star image is saturated on shortest UIT exposure. Convolution of UIT B5 bandpass with IUE spectrum SWP22007 gives m(162)=8.86



Table 3. SMC HII Region Ha and FUV Fluxes

#	DEM #	KH H $\alpha$		FUV Stellar		FUV Aperture		“Sky” Flux <sup>c</sup>
		Flux <sup>a</sup>	$\sigma$	Flux <sup>b</sup>	$\sigma$	Flux <sup>b</sup>	$\sigma$	
1	14	5.00	1.00	1.047	0.081	2.397	0.074	0.022
2	15	0.70	0.30	1.067	0.101	1.665	0.061	0.015
3	17	1.70	0.20	0.190	0.016	0.559	0.036	0.006
4	18	4.70	0.70	1.158	0.105	1.781	0.061	0.015
5	20	2.90	0.50	0.755	0.048	1.987	0.063	0.015
6	22	2.00	0.20	0.498	0.032	1.059	0.036	0.006
7	23	8.40	1.00	0.253	0.015	1.017	0.041	0.006
8	24	2.80	0.30	0.146	0.010	0.747	0.036	0.006
9	30	2.90	0.30	0.405	0.033	1.217	0.037	0.006
10	31	2.50	0.30	0.201	0.013	0.378	0.025	0.002
11	32	40.00	4.00	6.202	0.463	11.814	0.107	0.040
12	35	1.30	0.20	1.362	0.085	4.246	0.084	0.030
13	36	0.90	0.20	1.793	0.108	4.655	0.085	0.030
14	37	10.00	1.50	1.978	0.116	4.825	0.085	0.030
15	40	4.20	0.50	0.779	0.050	1.446	0.037	0.006
16	42	3.20	0.40	0.364	0.024	0.943	0.036	0.006
17	43	6.50	0.70	0.545	0.032	1.177	0.037	0.006
18	45	11.50	1.20	0.589	0.049	1.203	0.050	0.010
19	46	2.30	0.30	0.720	0.033	2.779	0.034	0.022
20	47	1.70	0.20	0.556	0.026	1.069	0.018	0.006
21	49	5.00	1.30	1.669	0.114	3.286	0.061	0.015
22	54	28.00	2.80	3.557	0.212	7.581	0.052	0.040
23	55	25.00	2.50	4.585	0.217	8.356	0.047	0.040
24	56	4.00	0.40	3.464	0.151	5.338	0.051	0.030
25	57	0.70	0.20	0.312	0.020	0.745	0.018	0.006
26	63	40.00	4.00	22.478	1.077	33.105	0.097	0.139
27	69	19.50	4.00	4.353	0.217	13.957	0.059	0.075
28	77	1.30	0.20	2.616	0.139	2.750	0.024	0.010
29	80	13.50	1.50	5.744	0.326	8.266	0.044	0.089
30	83	0.40	0.20	0.670	0.039	0.550	0.009	0.006
31	84	0.20	0.20	0.379	0.024	0.276	0.006	0.002
32	85	1.30	0.30	2.562	0.156	2.369	0.022	0.030
33	86	1.30	0.30	2.145	0.126	2.465	0.022	0.030
34	90	1.70	0.50	2.534	0.129	2.916	0.015	0.040

Table 3—Continued

#	DEM #	KH H $\alpha$		FUV Stellar		FUV Aperture		“Sky” Flux <sup>c</sup>
		Flux <sup>a</sup>	$\sigma$	Flux <sup>b</sup>	$\sigma$	Flux <sup>b</sup>	$\sigma$	
35	93	0.80	0.20	1.575	0.091	1.552	0.016	0.015
36	94	1.30	0.20	1.603	0.080	1.653	0.016	0.015
37	98	2.00	0.20	0.387	0.014	0.383	0.004	0.002
38	100	0.70	0.20	0.299	0.017	0.353	0.005	0.006
39	101	0.60	0.20	0.363	0.023	0.387	0.005	0.006
40	102	3.40	0.40	1.410	0.070	1.251	0.009	0.010
41	103	155.00	16.00	29.339	1.747	93.790	32.747	0.158
42	111	1.20	0.20	0.521	0.037	0.491	0.006	0.006

<sup>a</sup> $\times 10^{11}$  erg (cm<sup>2</sup> s)<sup>-1</sup>

<sup>b</sup> $\times 10^{12}$  erg (cm<sup>2</sup>Å s)<sup>-1</sup>

<sup>c</sup> $\times 10^{12}$  erg (cm<sup>2</sup>Å s)<sup>-1</sup> . Estimated sky flux contributed by non-SMC background in the apertures, as described in the text.

This figure "fig1.gif" is available in "gif" format from:

<http://arxiv.org/ps/astro-ph/9612152v1>

This figure "fig2a.gif" is available in "gif" format from:

<http://arxiv.org/ps/astro-ph/9612152v1>

This figure "fig2b.gif" is available in "gif" format from:

<http://arxiv.org/ps/astro-ph/9612152v1>

This figure "fig6.gif" is available in "gif" format from:

<http://arxiv.org/ps/astro-ph/9612152v1>